

Static and free vibration behaviour of orthotropic elliptic paraboloid shells

Kutlu Darılmaz*

Department of Civil Engineering, Istanbul Technical University, 34469, Maslak, Istanbul, Turkey

(Received August 06, 2016, Revised December 02, 2017, Accepted January 02, 2017)

Abstract. In this paper the influence of aspect ratio, height ratio and material angle on static and free vibration behaviour of orthotropic elliptic paraboloid shells is studied by using a four-node hybrid stress finite element. The formulation of the element is based on Hellinger-Reissner variational principle. The element is developed by combining a hybrid plane stress element and a hybrid plate element. A parametric study is carried out for static and free vibration response of orthotropic elliptic paraboloid shells with respect to displacements, internal forces, fundamental frequencies and mode shapes by varying the aspect and height ratios, and material angle.

Keywords: elliptic paraboloid shell; assumed stress hybrid element; finite element; static analysis; free vibration

1. Introduction

Elliptic paraboloid shells have been widely used in important aerospace, marine, and structural systems. Therefore, there are real, practical needs for researching this type of structures.

There have been extensive research carried out in the past years to investigate the behavior and design of circular shell structures but the literature on the analysis of non-circular shells is limited when compared with circular shells. The readers are referred to the following papers for analysis of non-circular shells. Suzuki *et al.* (1996) presented an exact solution procedure for analyzing free vibrations of laminated composite, noncircular thick cylindrical shells, and discussed the effects of shear deformation and rotary inertia by comparing the results from the present theory with those from the classical laminated shell theory. Ganapathi and Haboussi (2003) studied the free vibration characteristics of thick laminated composite non-circular cylindrical shells by using higher-order theory, and investigated the influences of length and thickness ratios, eccentricity parameters, ply-angles and number of layers on the free vibration characteristics. Sambandam *et al.* (2003) studied the elastic buckling characteristics of laminated cross-ply elliptical cylindrical shells under axial compression, and examined the combined influence of higher-order shear deformation, shell geometry and elliptical cross-sectional parameter, and lay-up on the buckling loads of elliptical cylindrical shells. Ganapathi *et al.* (2004) investigated the free flexural vibration characteristics of anisotropic laminated angle-ply elliptical cylindrical shells using finite element approach based on first-order shear deformation theory, and studied the effects of shell geometry, cross-sectional properties, lap-up and

ply-angle on the natural frequencies pertaining to different types of modes of vibrations. Patel *et al.* (2005), analyzed free vibration characteristics of functionally graded elliptical cylindrical shells using finite element formulated based on the theory with higher-order through the thickness approximations of both in-plane and transverse displacements, and carried out parametric studies to study the influences of non-circularity, radius-to-thickness ratio, material composition and material profile index on the free vibration frequencies and mode shape characteristics. Lo and Hyer (2012) used Hamilton's principle coupled with the Rayleigh-Ritz technique to compute the fundamental frequencies of simply supported thin-walled fiber-reinforced composite cylinders with elliptical cross sections, and investigated the dependence of the fundamental frequency on fiber angle, cross-sectional geometry, cylinder circumference, and cylinder length. Kazemi *et al.* (2012) investigated the elastic buckling behavior of piezocomposite elliptical cylindrical shell, and presented a serendipity quadrilateral eight-node element. They examined the influences of elliptical cross-sectional parameter and displacement feedback gain values on the critical buckling loads of elliptical cylindrical shells. Zhang *et al.* (2014) investigated the effects of stiffening rings on the dynamic properties of hyperboloidal cooling towers. Kang (2015) presented a three dimensional method of analysis for determining the free vibration frequencies of hyperboloidal shells free at the top edge and clamped at the bottom edge. Bochkarev *et al.* (2015) studied the solution of three-dimensional problems of natural vibrations and stability of loaded cylindrical shells with circular and arbitrary cross sections containing a quiescent ideal compressible fluid.

Concerning the analysis of elliptic paraboloid type of non-circular shells, there is a much smaller amount of work. One of the earliest works in element formulations for the analysis of elliptical parabolic shells was reported by Aass (1963) who applied it to elliptic paraboloid shells.

*Corresponding author, Ph.D., Professor,
E-mail: darilmazk@itu.edu.tr

Mohraz and Schnobrich (1966) studied the analysis of shallow shell structures including elliptic paraboloid shells by a discrete element system. Chun *et al.* (2009) presented a shear deformable four-noded finite element based on a hybrid/mixed assumed stress for the analysis of anisotropic laminated elliptical and parabolic shells, and conducted a parametric study of anisotropic elliptical and parabolic shells of various configurations to investigate the effects of aspect and height ratios as well as layer lay-up schemes.

It is well known that some of general shaped shells have been quite successfully solved by flat-shell elements of rectangular or quadrilateral shapes. For practical purposes, the behavior of a curved surface can be reasonably well approximated by using small flat elements. The flat element approximation also allows an easy coupling with the edge beams which sometimes difficult to implement in the curved element formulation.

In this paper, a flat shell element which is a combination of membrane element and a plate element is used, based on the classical hybrid stress method which was first developed by Pian (1964). The element is generated by a combination of a hybrid plane stress element with drilling d.o.f. and a hybrid plate element. The validity and efficiency of the presented element can be found in previous studies of the author, Darılmaz (2007, 2012). By using this element, influence of aspect and height ratios and material angle on static and vibration behaviour of orthotropic elliptic paraboloid shells is studied.

2. Element stiffness formulation

The assumed-stress hybrid method is based on the independent prescriptions of stresses within the element and displacements on the element boundary. The element stiffness matrix is obtained using Hellinger-Reissner variational principle. The Hellinger-Reissner functional of linear elasticity allows displacements and stresses to be varied separately. This establishes the master fields. Two slave strain fields appear, one coming from displacements and one from stresses.

The Hellinger-Reissner functional can be written as

$$\Pi_{RH} = \int_V \{\sigma\}^T [D] \{u\} dV - \frac{1}{2} \int_V \{\sigma\}^T [S] \{\sigma\} dV \quad (1)$$

where $\{\sigma\}$ is the stress vector, $[S]$ is the compliance matrix relating strains, $\{\varepsilon\}$, to stress ($\{\varepsilon\} = [S]\{\sigma\}$), $[D]$ is the differential operator matrix corresponding to the linear strain-displacement relations ($\{\varepsilon\} = [D]\{u\}$) and V is the volume of structure.

The approximation for stresses and displacements can now be incorporated in the functional. The stress field is described in the interior of the element as

$$\{\sigma\} = [P]\{\beta\} \quad (2)$$

and a compatible displacement field is described by

$$\{u\} = [N]\{q\} \quad (3)$$

where $[P]$ and $[N]$ are matrices of stress and displacement interpolation functions, respectively, and $\{\beta\}$ and $\{q\}$ are the unknown stress and nodal displacement parameters, respectively. Intra-element equilibrating stresses and compatible displacements are independently interpolated. Since stresses are independent from element to element, the stress parameters are eliminated at the element level and a conventional stiffness matrix results. This leaves only the nodal displacement parameters to be assembled into the global system of equations.

Substituting the stress and displacement approximations Eq. (2), Eq. (3) in the functional Eq. (1) yields

$$\Pi_{RH} = [\beta]^T [G][q] - \frac{1}{2} [\beta]^T [H][\beta] \quad (4)$$

where

$$[H] = \int_V [P]^T [S][P] dV \quad (5)$$

$$[G] = \int [P]^T ([D][N]) dV \quad (6)$$

Now imposing stationary conditions on the functional with respect to the stress parameters $\{\beta\}$ gives

$$[\beta] = [H]^{-1} [G] [q] \quad (7)$$

Substitution of $\{\beta\}$ in Eq. (4), the functional reduces to

$$\Pi_{RH} = \frac{1}{2} [q]^T [G]^T [H]^{-1} [G][q] = \frac{1}{2} [q]^T [K][q] \quad (8)$$

$$[K] = [G]^T [H]^{-1} [G] \quad (9)$$

is recognized as a stiffness matrix.

The solution of the system yields the unknown nodal displacements $\{q\}$. After $\{q\}$ is determined, element stresses or internal forces can be recovered by use of Eq. (7) and Eq. (2). Thus

$$\{\sigma\} = [P][H]^{-1} [G]\{q\} \quad (10)$$

3. Governing equations

Consider an elliptic paraboloid shell of uniform thickness which the orthotropic material property may be arbitrarily oriented at an angle ϕ with reference to the x -axis of the local coordinate system Fig. 1.

The stress-strain relation with respect to x , y and z axes can be written as

$$\begin{Bmatrix} \sigma_x \\ \sigma_y \\ \tau_{xy} \end{Bmatrix} = \begin{bmatrix} \bar{\Omega}_{11} & \bar{\Omega}_{12} & \bar{\Omega}_{16} \\ \bar{\Omega}_{12} & \bar{\Omega}_{22} & \bar{\Omega}_{26} \\ \bar{\Omega}_{16} & \bar{\Omega}_{26} & \bar{\Omega}_{66} \end{bmatrix} \begin{Bmatrix} \varepsilon_x \\ \varepsilon_y \\ \gamma_{xy} \end{Bmatrix} \quad \text{or} \quad (11)$$

$$\{\sigma\} = [\bar{\Omega}_{ij}]\{\varepsilon\} \quad (i, j = 1, 2, 6)$$

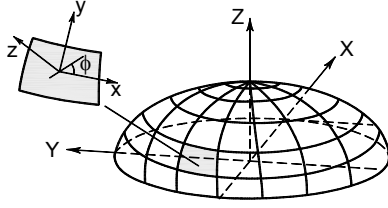


Fig. 1 Global and local axis of elliptic paraboloid shell

$$\begin{cases} \tau_{xz} \\ \tau_{yz} \end{cases} = \begin{bmatrix} \bar{\Omega}_{44} & \bar{\Omega}_{45} \\ \bar{\Omega}_{45} & \bar{\Omega}_{55} \end{bmatrix} \begin{cases} \gamma_{xz} \\ \gamma_{yz} \end{cases} \quad \text{or} \quad (12)$$

$$\{\tau\} = [\bar{\Omega}_{ij}] \{\gamma\} \quad (i, j = 4, 5)$$

$[\bar{\Omega}_{ij}]$ in Eqs. (11) and (12) is defined as

$$[\bar{\Omega}_{ij}] = [T_1]^{-1} [\Omega_{ij}] [T_1]^{-T} \quad (i, j = 1, 2, 6) \quad (13)$$

$$[\bar{\Omega}_{ij}] = [T_2]^{-1} [\Omega_{ij}] [T_2] \quad (i, j = 4, 5) \quad (14)$$

in which

$$[T_1] = \begin{bmatrix} \cos^2 \phi & \sin^2 \phi & 2 \sin \phi \cos \phi \\ \sin^2 \phi & \cos^2 \phi & -2 \sin \phi \cos \phi \\ -\sin \phi \cos \phi & \sin \phi \cos \phi & \cos^2 \phi - \sin^2 \phi \end{bmatrix} \quad (15)$$

$$[T_2] = \begin{bmatrix} \cos \phi & -\sin \phi \\ \sin \phi & \cos \phi \end{bmatrix} \quad (16)$$

$$[\Omega_{ij}] = \begin{bmatrix} \Omega_{11} & \Omega_{12} & 0 \\ \Omega_{12} & \Omega_{22} & 0 \\ 0 & 0 & \Omega_{66} \end{bmatrix} \quad (i, j = 1, 2, 6), \quad (17)$$

$$[\Omega_{ij}] = \begin{bmatrix} \Omega_{44} & 0 \\ 0 & \Omega_{55} \end{bmatrix} \quad (i, j = 4, 5)$$

$$\Omega_{11} = \frac{E_1}{I - \nu_{12}\nu_{21}} \quad \Omega_{12} = \frac{\nu_{12}E_2}{I - \nu_{12}\nu_{21}} \quad \Omega_{22} = \frac{E_2}{I - \nu_{12}\nu_{21}} \quad (18a)$$

$$\Omega_{66} = G_{12} \quad \Omega_{44} = G_{13} \quad \Omega_{55} = G_{23} \quad (18b)$$

$$G_{ij} = \frac{\sqrt{E_{ij}E_{ji}}}{2(I + \sqrt{\nu_{ij}\nu_{ji}})} \quad (i, j = 1, 2, 3) \quad (18c)$$

The stress resultants are given by

$$\begin{bmatrix} N_x & M_x \\ N_y & M_y \\ N_{xy} & M_{xy} \end{bmatrix} = \int_{-h/2}^{h/2} \begin{bmatrix} \sigma_x \\ \sigma_y \\ \tau_{xy} \end{bmatrix} [I \quad z] dz \quad (i, j = 1, 2, 3) \quad (19a)$$

$$\begin{bmatrix} Q_x \\ Q_y \end{bmatrix} = \int_{-h/2}^{h/2} \begin{bmatrix} \tau_{xz} \\ \tau_{yz} \end{bmatrix} dz \quad (i, j = 1, 2, 3) \quad (19b)$$

From Eqs. (19a) and (19b) the constitutive equations of the elliptic paraboloid shell are obtained as

$$\{F\} = [E] \{\chi\} \quad (i, j = 1, 2, 3) \quad (20)$$

where

$$\{F\} = \{N_x, N_y, N_{xy}, M_x, M_y, M_{xy}, Q_x, Q_y\} \quad (21)$$

$$\{\chi\} = \{\varepsilon_x, \varepsilon_y, \gamma_{xy}, \kappa_x, \kappa_y, \kappa_{xy}, \gamma_{xz}, \gamma_{yz}\} \quad (22)$$

The elasticity matrix can be expressed as

$$[E] = \begin{bmatrix} [A_{ij}] & [B_{ij}] & 0 \\ [B_{ij}] & [C_{ij}] & 0 \\ 0 & 0 & [D_{ij}] \end{bmatrix} \quad (23)$$

in which

$$[A_{ij}] = \int_{-h/2}^{h/2} [\bar{\Omega}_{ij}] dz, \quad [B_{ij}] = \int_{-h/2}^{h/2} [\bar{\Omega}_{ij}] z dz, \quad (24a)$$

$$[C_{ij}] = \int_{-h/2}^{h/2} [\bar{\Omega}_{ij}] z^2 dz \quad (i, j = 1, 2, 6)$$

$$[D_{ij}] = \int_{-h/2}^{h/2} [\bar{\Omega}_{ij}] dz \quad (i, j = 4, 5) \quad (24b)$$

4. The hybrid stress element

The element is generated by a combination of a hybrid membrane element and a hybrid plate element.

4.1 Membrane component of the element with drilling degree of freedom

Generally membrane elements have two translational d.o.f (u, v) per node but the need for membrane elements with a drilling degree of freedom arises in many engineering problems. A drilling rotation is defined as inplane rotation about the axis normal to the plane of element. This type of element is useful in solving folded plate structures and provides an easy coupling with edge beams which have six d.o.f per node. Inclusion of a drilling degree of freedom gives also the improved behavior of the element (Allman 1984). The possibility of membrane elements with drilling d.o.f was opened by Allman (1984), Bergan and Felippa (1985). The concept has been further elaborated by many other researchers (Cook 1986, MacNeal and Harder 1988, Yunus *et al.* 1989, Ibrahimbegovic *et al.* 1990, Choi and Lee 1996) for more improved elements.

Formulation of drilling d.o.f for the present element is based on the procedure given by Yunus *et al.* (1989). The displacement fields are expressed in terms of translational and rotational d.o.f.'s at the corner nodes only.

The membrane displacement field for the 4-node element is derived from an 8-node element, Fig. 2.

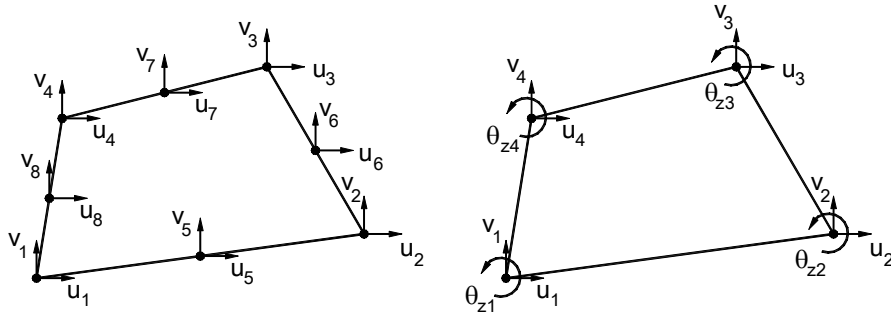


Fig. 2 Displacements for (a) 8-node membrane; (b) 4-node membrane

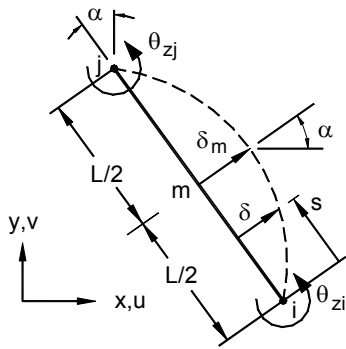


Fig. 3 Side displacement produced by drilling degrees of freedoms θ_{zi} and θ_{zj}

Rotational d.o.f. are associated with parabolic displaced shapes of element sides. In Fig. 3, rotational d.o.f. θ_{zi} and θ_{zj} are shown at nodes i and j of the element side of length L .

δ can be regarded as quadratic in side-tangent coordinates. θ_{zi} and θ_{zj} produce the edge normal displacement δ and midside value δ_m

$$\delta = \frac{s(L-s)}{2L}(\theta_{zi} - \theta_{zj}) \quad \delta_m = \frac{L}{8}(\theta_{zi} - \theta_{zj}) \quad (25)$$

The x and y components of δ are $\delta \cos \alpha$ and $\delta \sin \alpha$. Therefore, after adding the contribution to displacement from nodes i and j , the total displacements u and v of a typical point on the edge are

$$\begin{Bmatrix} u \\ v \end{Bmatrix} = \frac{L-s}{L} \begin{Bmatrix} u_i \\ v_i \end{Bmatrix} + \frac{s}{L} \begin{Bmatrix} u_j \\ v_j \end{Bmatrix} + \frac{(L-s)s}{2L}(\theta_{zj} - \theta_{zi}) \begin{Bmatrix} \cos \alpha \\ \sin \alpha \end{Bmatrix} \quad (26)$$

Side 1-5-2 of the element, Fig. 2 d.o.f. at node 5 are related to d.o.f. at nodes 1 and 2 of the element. By evaluating Eq. (2) with $s = L/2$ with $i = 1, j = 2, L \cos \alpha = y_2 - y_1$ and $L \sin \alpha = x_1 - x_2$, yields

$$\begin{Bmatrix} u_5 \\ v_5 \end{Bmatrix} = \frac{1}{2} \begin{Bmatrix} u_1 \\ v_1 \end{Bmatrix} + \frac{1}{2} \begin{Bmatrix} u_2 \\ v_2 \end{Bmatrix} + \frac{(\theta_{zj} - \theta_{zi})}{8} \begin{Bmatrix} y_2 - y_1 \\ x_1 - x_2 \end{Bmatrix} \quad (27)$$

After doing the same for d.o.f. at nodes 6, 7 and 8 d.o.f. in Figs. 1(b) and (c) by the transformation, the complete relation can be written

$$\{u_1 \ v_1 \ u_2 \ v_2 \ \dots \ u_8 \ v_8\}^T = [T]_{16 \times 12} \{q\}_{membrane}^T \quad (28)$$

where

$$\{q\}_{membrane} = \{u_1 \ v_1 \ \theta_{z1} \ u_2 \ v_2 \ \theta_{z2} \ u_3 \ v_3 \ \theta_{z3} \ u_4 \ v_4 \ \theta_{z4}\} \quad (29)$$

So the midside nodal displacements can be written in terms of the corner nodal displacements and rotations and the displacement field for the 4-node, twelve d.o.f. membrane element can be derived from an 8-node membrane element. This is done through the use of the transformation matrix $[T]$. The form of $[T]$ is given in Appendix 1.

The biggest difficulty in deriving hybrid finite elements seems to be the lack of a rational methodology for deriving stress terms, Feng *et al.* (1997). It is recognized that the number of stress modes m in the assumed stress field should satisfy

$$m \geq n - r \quad (30)$$

with n the total number of nodal displacements, and r the number of rigid body modes in an element. If Eq. (30) is not satisfied, use of too few coefficients in $\{\beta\}$, the rank of the element stiffness matrix will be less than the total degrees of deformation freedom and the numerical solution of the finite element model will not be stable and produces on element with one or more mechanism.

Increasing the number of β 's by adding stress modes of higher-order term, each extra term will add more stiffness and stiffens the element, Pian and Chen (1983), Punch and Atluri (1984), Darılmaz and Kumbasar (2006).

The assumed stress field for the membrane part which satisfies the equilibrium conditions for zero body forces and avoid rank deficiency is given as

$$\begin{aligned} N_x &= \beta_1 + \beta_2 x + \beta_3 y + \beta_4 x^2 + \beta_5 xy + \beta_6 y^2 \\ N_y &= \beta_4 y^2 + \beta_7 + \beta_8 x + \beta_9 y + \beta_{10} x^2 + \beta_{11} xy \\ N_{xy} &= -\beta_2 y - 2\beta_4 xy - \beta_5 y^2 / 2 - \beta_9 x - \beta_{11} x^2 / 2 + \beta_{12} \end{aligned} \quad (31)$$

4.2 Plate component of the element

The flexural component of the element is identical to that of the plate bending element presented by the author, Darılmaz (2005), and corresponds to the Mindlin/Reissner plate theory. Only the assumed stress field which satisfies

the equilibrium conditions for the plate part is given here

$$\begin{aligned}
 M_x &= \beta_1 + \beta_4 y + \beta_6 x + \beta_8 xy \\
 M_y &= \beta_2 + \beta_5 x + \beta_7 y + \beta_9 xy \\
 M_{xy} &= \beta_3 + \beta_{10} x + \beta_{11} y + \beta_{12} x^2 / 2 + \beta_{13} y^2 / 2 \\
 Q_x &= \beta_6 + \beta_{11} + \beta_8 y + \beta_{13} y \\
 Q_y &= \beta_7 + \beta_{10} + \beta_9 x + \beta_{12} x
 \end{aligned}
 \tag{32}$$

The nodal displacements for the plate are chosen as

$$\begin{aligned}
 \{q\}_{plate} = \{ & w_1 \quad \theta_{x1} \quad \theta_{y1} \quad w_2 \quad \theta_{x2} \quad \theta_{y2} \\
 & \theta_{y2} \quad w_3 \quad \theta_{x3} \quad \theta_{y3} \quad w_4 \quad \theta_{x4} \quad \theta_{y4} \}
 \end{aligned}
 \tag{33}$$

The combination of membrane and plate element yields the element which has 6 d.o.f per node and totally 24 d.o.f.

5. Element mass matrix

The problem of determination of the natural frequencies of vibration of a plate reduces to the solution of the standard eigenvalue problem $[K] - \omega^2[M] = 0$, where ω is the natural circular frequency of the system. Making use of the conventional assemblage technique of the finite element method with the necessary boundary conditions, the system matrix $[K]$ and the mass matrix $[M]$ for the entire structure can be obtained.

Element mass matrix is derived from the kinetic energy expression.

$$E_k = \frac{1}{2} \int_A \{\dot{q}\}^T [R] \{\dot{q}\} dA \tag{34}$$

where $\{\dot{q}\}$ denotes the velocity components and $[R]$ is the inertia matrix.

The nodal and generalized velocity vectors are related with the help of shape functions

$$\{\dot{q}\} = \sum_{i=1}^4 [N] \{\dot{q}_i\} \tag{35}$$

Substituting the velocity vectors in the kinetic energy, Eq. (34) yields the mass matrix of an element.

$$E_k = \frac{1}{2} \int_A \{\dot{q}_i\}^T [N]^T [R] [N] \{\dot{q}_i\} dA \tag{36}$$

$$E_k = \frac{1}{2} \int_A \{\dot{q}_i\}^T [m] \{\dot{q}_i\} dA \tag{37}$$

where $[m]$ is the element consistent mass matrix and is given by

$$[m] = \int_A [N]^T [R] [N] dA \tag{38}$$

6. Numerical study

A parametric study is carried out to investigate the influence of aspect and height ratios, and material angle on

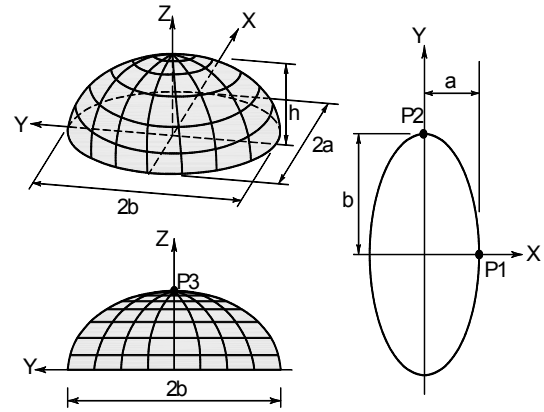


Fig. 4 Geometry of elliptic paraboloid shell

static and free vibration behaviour of orthotropic elliptic paraboloid shells. A simply supported orthotropic elliptic paraboloid shell is considered with the coordinates x along the circumferential direction, y along the meridian direction and z along the thickness direction, Fig. 4. Material properties are chosen as, $E_1 = 60.7 \times 10^9 \text{ N/m}^2$, $E_2 = 24.8 \times 10^9 \text{ N/m}^2$, $G_{12} = G_{13} = G_{23} = 12 \times 10^9 \text{ N/m}^2$, $\nu_{12} = \nu_{21} = 0.23$, $\rho = 1300 \text{ kg/m}^3$ where E_1 and E_2 are the modulus of elasticity along x and y axes of element, G_{ij} is the shear modulus and ν_{ij} is Poisson's ratio, respectively.

Displacements and internal forces are investigated with variations in aspect ratios, height ratios and material angle. The aspect ratio, b/a , of elliptical shell is taken as the ratio of the radius length of Y -axis to that of X -axis. Whereas, the height ratio h/b , of elliptical shell is taken as the radius length of Z -axis divide into that of Y -axis.

To obtain the optimal mesh for the problem a convergence analysis is carried out, and 60 elements in circumferential direction, 16 elements in meridional direction is used.

The influence of aspect ratio b/a of elliptical paraboloid shells is analysed by varying the aspect ratio ($b/a = 1.0, 2.0$ and 4.0). Displacement and internal forces are investigated for different height ratio values ($h/b = 0.25, 0.50$ and 1.0). The calculated non-dimensional axial forces \bar{N}_y and \bar{N}_x are given in Table 1, Table 2 for points P1 and P2 (shown in Fig. 4). It is observed that generally both \bar{N}_y and \bar{N}_x values are decreasing with the increasing aspect ratio (b/a). For $b/a \geq 2$, it was found that increase in the height ratio (h/b) results in greater increase in \bar{N}_y and \bar{N}_x values. For example for $b/a = 4$, \bar{N}_y increased 53% for $\phi = 0^\circ$. Furthermore, it can be observed that \bar{N}_y is less sensitive to material angle than \bar{N}_x .

In Table 3 and 4 non-dimensional moment values, \bar{M}_x and \bar{M}_y , are given for vertex point P3 along X and Y axis. It is observed that generally both \bar{M}_x and \bar{M}_y values are decreasing with the increasing aspect ratio (b/a). Furthermore, it is noticed that material angle and height ratio (h/b) can significantly effect the moment values at vertex point. For $b/a \leq 2$, with decrease in height ratio results increase in \bar{M}_x and \bar{M}_y values due to the increasing effect of flexural behaviour in the vicinity of vertex point. For example for $b/a = 1$, \bar{M}_x increased 519% for $\phi = 0^\circ$.

Table 1 Non-dimensional axial force $\bar{N}_y = N_y/bq$ ($\times 10^3$) for elliptic paraboloid shell

Point	h/b	$b/a = 1$			$b/a = 2$			$b/a = 4$		
		0.25	0.5	1.0	0.25	0.5	1.0	0.25	0.5	1.0
	\emptyset									
P1	0°	-1146.9	-840.6	-947.3	-680.9	-681.4	-912.0	-396.6	-556.4	-847.1
	45°	-1036.3	-860.1	-950.1	-710.9	-703.0	-913.5	-394.5	-557.9	-832.5
	90°	-1080.4	-796.6	-904.1	-702.0	-727.1	-984.6	-391.5	-596.3	-951.6
P2	0°	-1146.9	-840.6	-947.3	-378.4	-412.0	-721.2	-165.6	-352.0	-731.4
	45°	-1036.3	-770.8	-886.3	-213.7	-272.7	-569.8	-65.2	-190.4	-489.8
	90°	-1080.4	-796.6	-904.1	-226.8	-317.4	-629.9	-77.3	-324.6	-755.4

Table 2 Non-dimensional axial force $\bar{N}_y = N_y/bq$ ($\times 10^3$) for elliptic paraboloid shell

Point	h/b	$b/a = 1$			$b/a = 2$			$b/a = 4$		
		0.25	0.5	1.0	0.25	0.5	1.0	0.25	0.5	1.0
	\emptyset									
P1	0°	-644.9	-472.9	-534.3	-378.4	-412.0	-721.2	-165.6	-352.0	-731.4
	45°	-352.2	-247.5	-272.7	-213.7	-272.7	-569.8	-65.2	-190.4	-489.8
	90°	-247.6	-182.5	-207.6	-226.8	-317.4	-629.9	-77.3	-324.6	-755.4
P2	0°	-644.9	-472.9	-534.3	-212.4	-232.0	-408.0	-93.2	-198.9	-413.7
	45°	-258.5	-194.2	-234.1	-15.8	-29.2	-103.9	-6.0	-16.9	-53.9
	90°	-247.6	-182.5	-207.6	-51.4	-72.6	-145.1	-17.5	-74.7	-174.4

Table 3 Non-dimensional moment $\bar{M}_y = M_y/b^2q$ ($\times 10^3$) at vertex point for elliptic paraboloid shell

	h/b	$b/a = 1$			$b/a = 2$			$b/a = 4$		
		0.25	0.5	1.0	0.25	0.5	1.0	0.25	0.5	1.0
	\emptyset									
X	0°	2.143	0.983	0.346	1.380	0.717	0.239	0.172	-0.083	-0.191
	45°	1.243	0.676	0.269	1.164	0.798	0.361	-0.089	-0.110	-0.154
	90°	-0.864	-0.147	0.002	0.317	0.560	0.306	-0.577	-0.804	-0.564
$/y$	0°	2.143	0.983	0.346	0.408	0.175	0.063	-0.053	-0.086	-0.079
	45°	1.243	0.676	0.269	0.191	0.120	0.062	-0.163	-0.166	-0.073
	90°	-0.864	-0.147	0.002	-0.085	0.008	0.015	-0.290	-0.364	-0.249

Table 4 Non-dimensional moment $\bar{M}_y = M_y/b^2q$ ($\times 10^3$) at vertex point for elliptic paraboloid shell

	h/b	$b/a = 1$			$b/a = 2$			$b/a = 4$		
		0.25	0.5	1.0	0.25	0.5	1.0	0.25	0.5	1.0
	\emptyset									
X	0°	4.128	1.894	0.667	2.446	1.339	0.513	0.654	0.238	0.017
	45°	1.243	0.676	0.269	1.175	0.817	0.396	0.174	0.164	0.038
	90°	-0.448	-0.077	0.001	0.239	0.327	0.198	-0.095	-0.135	-0.075
$/y$	0°	4.128	1.894	0.667	0.915	0.373	0.076	-0.282	-0.360	-0.351
	45°	1.243	0.676	0.269	0.267	0.166	0.066	-0.418	-0.418	-0.262
	90°	-0.448	-0.077	0.001	-0.101	0.023	0.009	-0.492	-0.615	-0.441

Non-dimensional vertical displacements along X and Y axis of elliptic paraboloid shells for various aspect ratios and height ratios are depicted in Figs. 5-7. For all cases the

maximum displacement is observed at the vertex point. This displacement is increasing with the decreasing height ratio (h/b). For aspect ratios different than $b/a = 1$, displacements

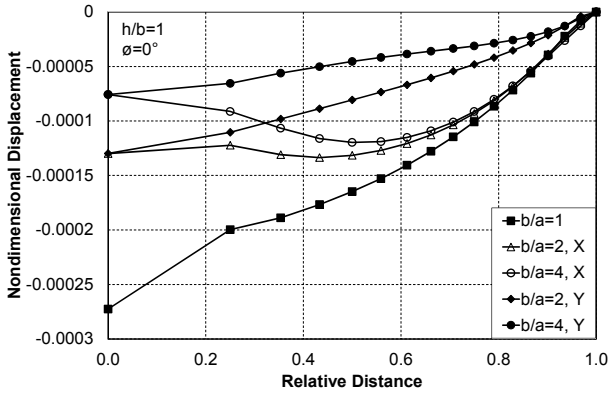


Fig. 5 Non-dimensional displacements $\bar{\delta} = \delta(E_1 h^3 / b^4 q)$ along X and Y axis ($h/b = 1, \varnothing = 0^\circ$)

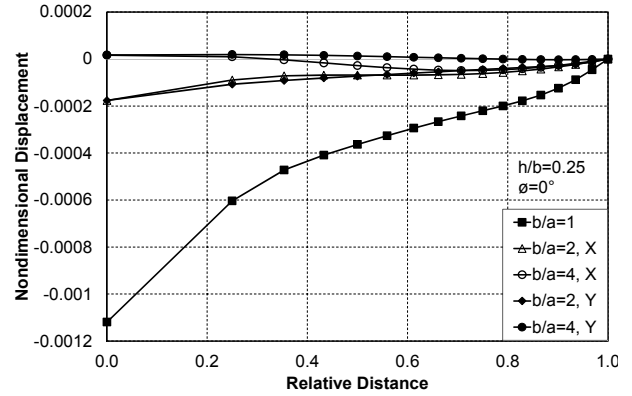


Fig. 7 Non-dimensional displacements along X and Y axis ($h/b = 0.25, \varnothing = 0^\circ$)

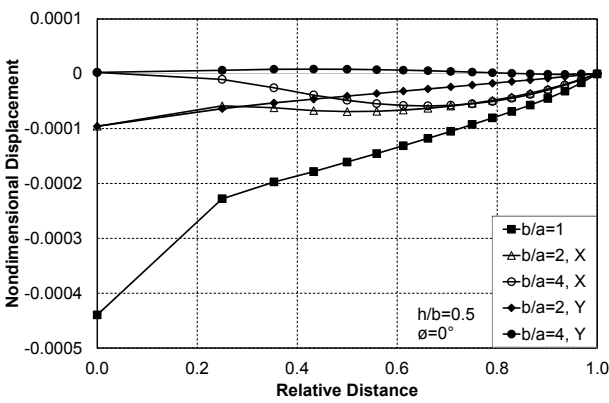


Fig. 6 Non-dimensional displacements $\bar{\delta} = \delta(E_1 h^3 / b^4 q)$ along X and Y axis ($h/b = 0.5, \varnothing = 0^\circ$)

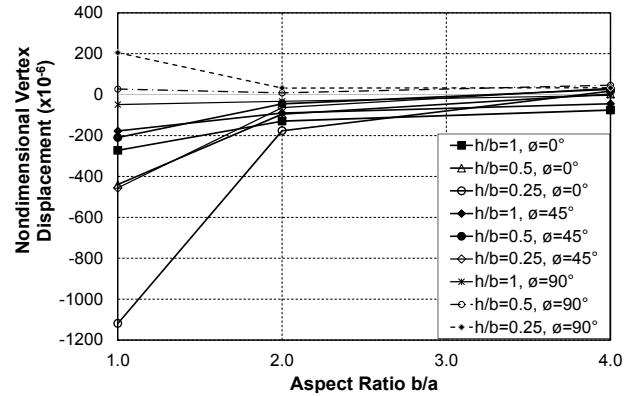


Fig. 8 Vertical displacement at the vertex point versus aspect ratio b/a

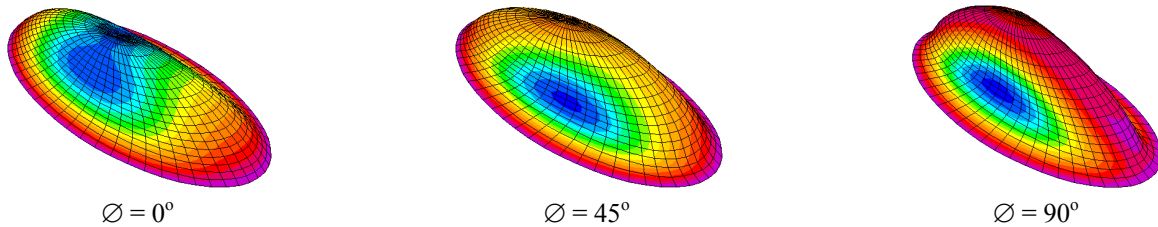


Fig. 9 Deformed shape of elliptic paraboloid shell for different material angles $b/a = 2, h/b = 0.5$

along X axis are larger than displacements along Y axis.

The vertical displacement at the vertex point $P3$ under uniform distributed load is obtained. The variation of non-dimensional vertex point displacement versus aspect ratio b/a is given in Fig. 8. It is observed that the vertical displacement at vertex point of elliptical paraboloid converged to a constant value for $b/a \geq 3$. In addition, it is noted that the behaviour is sensitive between aspect ratios 1.0 and 2.0.

The magnitude of displacements seems mostly related with the bending stiffness along meridian axis of the elliptical paraboloid shell. In Fig. 8 it can be observed that in case when material angle lowers the bending stiffness, displacements are increasing. Additionally material angle can effect the direction of displacement. An interesting contrast is observed with vertex displacement for $h/b =$

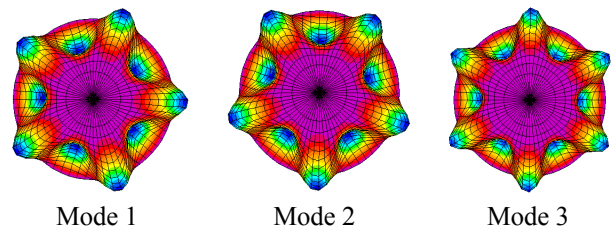


Fig. 10 First three modes of the elliptic paraboloid shell ($b/a = 1, h/b = 1, \varnothing = 0^\circ$)

0.25, $h/b = 0.5$ and $\varnothing = 90^\circ$, under vertical distributed loads the vertex displacement is in upward direction, Fig. 9.

To investigate the dynamic characteristics of elliptic paraboloid shells non-dimensional natural frequencies are

Table 5 Non-dimensional natural frequencies for elliptic paraboloid shell $[\bar{\omega} = \omega b \sqrt{\rho(1-\nu_{21}^2)/E_1}]$ for elliptic paraboloid shell

\emptyset	Mode	$b/a = 1$			$b/a = 2$			$b/a = 4$		
		$h/b = 0.25$	$h/b = 0.5$	$h/b = 1.0$	$h/b = 0.25$	$h/b = 0.5$	$h/b = 1.0$	$h/b = 0.25$	$h/b = 0.5$	$h/b = 1.0$
	0°	0.313	0.435	0.346	0.428	0.486	0.300	0.432	0.326	0.194
P1	45°	0.338	0.435	0.346	0.462	0.491	0.300	0.464	0.332	0.199
	90°	0.338	0.442	0.347	0.489	0.510	0.301	0.614	0.389	0.206
	0°	0.318	0.451	0.361	0.380	0.416	0.300	0.381	0.295	0.185
P2	45°	0.318	0.451	0.361	0.400	0.432	0.302	0.472	0.298	0.189
	90°	0.324	0.453	0.361	0.465	0.481	0.306	0.629	0.394	0.210
		0.335	0.480	0.391	0.365	0.407	0.308	0.390	0.297	0.186
P3		0.335	0.480	0.391	0.407	0.429	0.310	0.519	0.299	0.187
		0.335	0.512	0.393	0.488	0.474	0.316	0.640	0.404	0.210

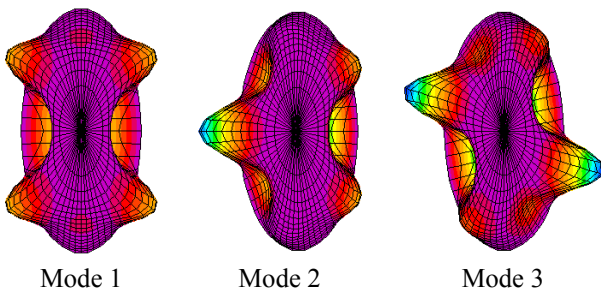


Fig. 11 First three modes of the elliptic paraboloid shell ($b/a = 2$, $h/b = 1$, $\emptyset = 0^\circ$)

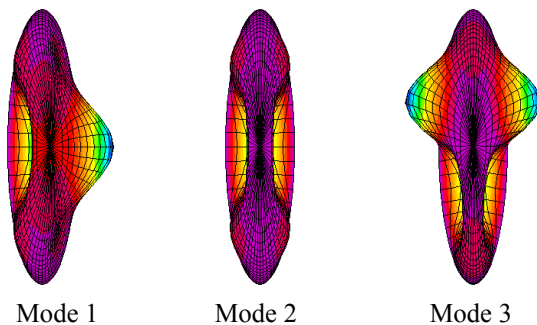


Fig. 12 First three modes of the elliptic paraboloid shell ($b/a = 4$, $h/b = 1$, $\emptyset = 0^\circ$)

obtained for different aspect ratios, height ratios and material angles, and the obtained values are given in Table 5. It is observed natural frequencies are more sensitive to aspect ratio and height ratio than material angle.

For the sake of brevity mode shapes are shown in Fig. 9-11 for aspect ratios $b/a = 1.0, 2.0, 4.0$, height ratio $h/b = 1$ and material angle $\emptyset = 0^\circ$ only.

6. Conclusions

An assumed stress hybrid finite element is used for the

static and free vibration analysis of elliptic paraboloid shells. A parametric study is carried out to investigate the influence of aspect ratio, height ratio and material angle on the static and dynamic behaviour of elliptic paraboloid shells. Based on the above parametric study, the following concluding remarks are made:

The vertical displacement at vertex point of elliptical paraboloid to a constant value for $b/a \geq 3$ and rapidly increasing for aspect ratio $b/a < 2$.

Generally an increase in height ratio increases axial forces and decreases moments.

Magnitude of displacements seems mostly related with the bending stiffness along meridian axis of the elliptical paraboloid shell.

Natural frequencies are more sensitive to aspect ratio and height ratio than material angle.

For the design of simply supported elliptic paraboloid shells, the variation of internal forces, displacements and frequencies with the aspect ratio a/b and height ratio h/b is presented in figures and tables that can be directly used in design practice.

References

- Aass, A. (1963), "A contribution to the bending theory of elliptic paraboloid shells", *IABSE*, **23**, p. 1.
- Allman, D.J. (1984), "A compatible triangular element including vertex rotations for plane elasticity problems", *Comp. Struct.*, **19**(1-2), 1-8.
- Bergan, P.G. and Felippa, C.A. (1985), "A triangular membrane element with rotational degrees of freedom", *Comp. Methods Appl. Mech. Eng.*, **50**(1), 25-69.
- Bochkarev, S.A., Lekomtsev, S.V. and Matveenkov, V.P. (2015), "Natural vibrations of loaded noncircular cylindrical shells containing a quiescent fluid", *Thin-Wall. Struct.*, **90**, 12-22.
- Choi, C.K. and Lee, W.H. (1996), "Versatile variable-node flat-shell element", *J. Eng. Mech.*, **122**(5), 432-441.
- Chun, K.S., Kassegne, S.K. and Wondimu, B.K. (2009), "Hybrid/mixed assumed stress element for anisotropic laminated elliptical and parabolic shells", *Finite Elem. Anal. Des.*, **45**(11), 766-781.
- Cook, R.D. (1986), "On the Allman triangle and a related quadri-

- lateral element”, *Comp. Struct.*, **22**(6), 1065-1067.
- Ganapathi, M. and Haboussi, M. (2003), “Free vibrations of thick laminated anisotropic non-circular cylindrical shells”, *Compos. Struct.*, **60**(2), 125-133.
- Darilmaz, K. (2005), “An assumed-stress finite element for static and free vibration analysis of Reissner-Mindlin plates”, *Struct. Eng. Mech., Int. J.*, **19**(2), 199-215.
- Darilmaz, K. (2007), “An assumed-stress hybrid element for static and free vibration analysis of folded plates”, *Struct. Eng. Mech., Int. J.*, **25**(4), 405-421.
- Darilmaz, K. (2012), “Stiffened orthotropic corner supported hypar shells: Effect of stiffener location, rise/span ratio and fiber orientation on vibration behavior”, *Steel Compos. Struct., Int. J.*, **12**(4), 275-289.
- Darilmaz, K. and Kumbasar, N. (2006), “An 8-node assumed stress hybrid element for analysis of shells”, *Comp. Struct.*, **84**(29), 1990-2000.
- Feng, W., Hoa, S.V. and Huang, Q. (1997), “Classification of stress modes in assumed stress fields of hybrid finite elements”, *Int. J. Num. Meth. Eng.*, **40**(23), 4313-4339.
- Ganapathi, M., Patel, B.P. and Patel, H.G. (2004), “Free flexural vibration behavior of laminated angle-ply elliptical cylindrical shells”, *Comp. Struct.*, **82**(6), 509-518.
- Ibrahimbegovic, A., Taylor, R.L. and Wilson, E.L. (1990), “A robust quadrilateral membrane finite element with drilling degrees of freedom”, *Int. J. Numer. Methods Eng.*, **30**(3), 445-457.
- Kang, J.H. (2015), “Vibration analysis of free-fixed hyperbolic cooling tower shells”, *Struct. Eng. Mech., Int. J.*, **55**(4), 785-799.
- Kazemi, E., Darvizeh, M., Darvizeh, A. and Ansari, R. (2012), “An investigation of the buckling behavior of composite elliptical cylindrical shells with piezoelectric layers under axial compression”, *Acta Mech.*, **223**(10), 2225-2242.
- Lo, H.C. and Hyer, M.W. (2012), “Fundamental natural frequencies of thin-walled elliptical composite cylinders”, *J. Compos. Mater.*, **46**(10), 1169-1190.
- MacNeal, R.H. and Harder, R.L. (1988), “A refined four-noded membrane element with rotational degrees of freedom”, *Compos. Struct.*, **28**(1), 75-84.
- Mohraz, B. and Schnobrich, W.C. (1966), “The analysis of shallow shell structures by a discrete element system”, Civil Engineering Studies, Structural Research Series No. 304.
- Patel, B.P., Gupta, S.S., Loknath, M.S. and Kadu, C.P. (2005), “Free vibration analysis of functionally graded elliptical cylindrical shells using higher-order theory”, *Compos. Struct.*, **69**(3), 259-270.
- Pian, T.H.H. (1964), “Derivation of element stiffness matrices by assumed stress distributions”, *AIAA J.*, **2**(7), 1333-1336.
- Pian, T.H.H. and Chen, D.P. (1983), “On the suppression of zero energy deformation modes”, *Int. J. Num. Meth. Eng.*, **19**(12), 1741-1752.
- Punch, E.F. and Atluri, S.N. (1984), “Development and testing of stable, isoparametric curvilinear 2 and 3-D hybrid stress elements”, *Comput. Meth. Appl. Mech. Eng.*, **47**, 331-356.
- Sambandam, C.T., Patel, B.P., Gupta, S.S., Munot, C.S. and Ganapathi, M. (2003), “Buckling characteristics of cross-ply elliptical cylinders under axial compression”, *Compos. Struct.*, **62**(1), 7-17.
- Suzuki, K., Shikanai, G. and Leissa, A.W. (1996), “Free vibrations of laminated composite non-circular thick cylindrical shells”, *Int. J. Solids Struct.*, **33**(27), 4079-4100.
- Yunus, S.M., Saigal, S. and Cook, R.D. (1989), “On improved hybrid finite elements with rotational degrees of freedom”, *Int. J. Numer. Meth. Eng.*, **28**(4), 785-800.
- Zhang, J.F., Chen, H., Ge, Y.J., Zhao, L. and Ke, S.T. (2014), “Effects of stiffening rings on the dynamic properties of hyperboloidal cooling towers”, *Struct. Eng. Mech., Int. J.*, **49**(5), 619-629.

CC

Appendix 1

$$[T] = \begin{bmatrix} 1 & 0 & 0 & 0 & 0 & 0 & 0 & 0 & 0 & 0 & 0 & 0 \\ 0 & 1 & 0 & 0 & 0 & 0 & 0 & 0 & 0 & 0 & 0 & 0 \\ 0 & 0 & 0 & 1 & 0 & 0 & 0 & 0 & 0 & 0 & 0 & 0 \\ 0 & 0 & 0 & 0 & 1 & 0 & 0 & 0 & 0 & 0 & 0 & 0 \\ 0 & 0 & 0 & 0 & 0 & 0 & 1 & 0 & 0 & 0 & 0 & 0 \\ 0 & 0 & 0 & 0 & 0 & 0 & 0 & 1 & 0 & 0 & 0 & 0 \\ 0 & 0 & 0 & 0 & 0 & 0 & 0 & 0 & 1 & 0 & 0 & 0 \\ 0 & 0 & 0 & 0 & 0 & 0 & 0 & 0 & 0 & 1 & 0 & 0 \\ \frac{1}{2} & 0 & \frac{(y_1 - y_2)}{8} & \frac{1}{2} & 0 & \frac{(y_2 - y_1)}{8} & 0 & 0 & 0 & 0 & 0 & 0 \\ 0 & \frac{1}{2} & \frac{(x_2 - x_1)}{8} & 0 & \frac{1}{2} & \frac{(x_1 - x_2)}{8} & 0 & 0 & 0 & 0 & 0 & 0 \\ 0 & 0 & 0 & \frac{1}{2} & 0 & \frac{(y_2 - y_3)}{8} & \frac{1}{2} & 0 & \frac{(y_3 - y_2)}{8} & 0 & 0 & 0 \\ 0 & 0 & 0 & 0 & \frac{1}{2} & \frac{(x_3 - x_2)}{8} & 0 & \frac{1}{2} & \frac{(x_2 - x_3)}{8} & 0 & 0 & 0 \\ 0 & 0 & 0 & 0 & 0 & 0 & \frac{1}{2} & 0 & \frac{(y_3 - y_4)}{8} & \frac{1}{2} & 0 & \frac{(y_4 - y_3)}{8} \\ 0 & 0 & 0 & 0 & 0 & 0 & 0 & \frac{1}{2} & \frac{(x_4 - x_3)}{8} & 0 & \frac{1}{2} & \frac{(x_3 - x_4)}{8} \\ \frac{1}{2} & 0 & \frac{(y_1 - y_4)}{8} & 0 & 0 & 0 & 0 & 0 & 0 & \frac{1}{2} & 0 & \frac{(y_4 - y_1)}{8} \\ 0 & \frac{1}{2} & \frac{(x_4 - x_1)}{8} & 0 & 0 & 0 & 0 & 0 & 0 & 0 & \frac{1}{2} & \frac{(x_1 - x_4)}{8} \end{bmatrix}$$

Appendix 2: Notation

E_1, E_2 : moduli of elasticity along x and y axes of element respectively

G_{12}, G_{13}, G_{23} : shear moduli of elasticity in x - y , x - z and y - z planes of element

x, y, z : element local axis

X, Y, Z : system global axis

ν_{12}, ν_{21} : Poisson ratio

$[D]$: differential operator matrix

$[E]$: elasticity matrix

$[G]$: nodal forces corresponding to assumed stress field

$[N]$: shape functions

$[R]$: inertia matrix

$[P]$: interpolation matrix for stress

$\{q\}, \{\dot{q}\}$: displacement and velocity components

$\{u\}$: displacements

$\{\beta\}$: stress parameters

$\{\sigma\}$: internal forces

Q_x, Q_y : internal shear forces per unit length

N_x, N_y, N_{xy} : membrane forces per unit length

M_x, M_y, M_{xy} : internal moments per unit length

\bar{N}_x : non-dimensional in-plane force along x local axis (circumferential force)

\bar{N}_y : non-dimensional in-plane force along y local axis (meridian in-plane force)

\bar{M}_x : non-dimensional moment about x local axis

\bar{M}_y : non-dimensional moment about y local axis

q : uniform distributed load

ρ : mass per unit volume

ω : natural circular frequency

ϕ : material angle in an element with reference to x -axis